

Article

Amperometric Miniaturised Portable Enzymatic Nanobiosensor for the Ultrasensitive Analysis of a Prostate Cancer Biomarker

Stefania Hroncekova¹, Lenka Lorencova¹, Tomas Bertok¹ , Michal Hires¹, Eduard Jane¹, Marek Bučko¹, Peter Kasak²  and Jan Tkac^{1,*} 

¹ Institute of Chemistry, Slovak Academy of Sciences, Dubravská Cesta 9, 845 38 Bratislava, Slovakia

² Center for Advanced Materials, Qatar University, Doha P.O. Box 2713, Qatar

* Correspondence: jan.tkac@savba.sk

Abstract: Screen-printing technology is a game changer in many fields including electrochemical biosensing. Two-dimensional nanomaterial MXene Ti₃C₂T_x was integrated as a nanoplatform to immobilise enzyme sarcosine oxidase (SOx) onto the interface of screen-printed carbon electrodes (SPCEs). A miniaturised, portable, and cost-effective nanobiosensor was constructed using chitosan as a biocompatible glue for the ultrasensitive detection of prostate cancer biomarker sarcosine. The fabricated device was characterised with energy-dispersive X-ray spectroscopy (EDX), electrochemical impedance spectroscopy (EIS) and cyclic voltammetry (CV). Sarcosine was detected indirectly via the amperometric detection of H₂O₂ formed during enzymatic reaction. The nanobiosensor could detect sarcosine down to 7.0 nM with a maximal peak current output at $4.10 \pm 0.35 \times 10^{-5}$ A using only 100 µL of a sample per measurement. The assay run in 100 µL of an electrolyte showed the first linear calibration curve in a concentration window of up to 5 µM with a slope of $2.86 \mu\text{A} \cdot \mu\text{M}^{-1}$, and the second linear calibration curve in the range of 5–50 µM with a slope of $0.32 \pm 0.01 \mu\text{A} \cdot \mu\text{M}^{-1}$ ($R^2 = 0.992$). The device provided a high recovery index of 92.5% when measuring an analyte spiked into artificial urine, and could be used for detection of sarcosine in urine for at least a period of 5 weeks after the preparation.

Keywords: biomarker; early diagnostics; MXene; nanobiosensor; prostate cancer; sarcosine; sarcosine oxidase; screen-printed electrodes; urine



Citation: Hroncekova, S.; Lorencova, L.; Bertok, T.; Hires, M.; Jane, E.; Bučko, M.; Kasak, P.; Tkac, J. Amperometric Miniaturised Portable Enzymatic Nanobiosensor for the Ultrasensitive Analysis of a Prostate Cancer Biomarker. *J. Funct. Biomater.* **2023**, *14*, 161. <https://doi.org/10.3390/jfb14030161>

Academic Editor: Zhuangqiang Gao

Received: 19 February 2023

Revised: 12 March 2023

Accepted: 14 March 2023

Published: 17 March 2023



Copyright: © 2023 by the authors. Licensee MDPI, Basel, Switzerland. This article is an open access article distributed under the terms and conditions of the Creative Commons Attribution (CC BY) license (<https://creativecommons.org/licenses/by/4.0/>).

1. Introduction

Prostate cancer (PCa) is one of the leading global causes of cancer death and the most frequent type of cancer diagnosed for men in 112 countries. Around 650,000 new patients are diagnosed with prostate cancer each year, and the incidence continues to rise [1,2]. Among PCa risk factors, the following are at the top of the list: age, race, genetic predispositions, and family history. PCa is also linked with other factors, including eating habits (a high consumption of saturated fat of animal origin and red meat, and a low intake of fruits, vegetables, vitamins, and coffee), being overweight, physical inactivity, inflammation, hyperglycaemia, infections, and exposure to hazardous chemicals and radiation [3,4]. Male androgenic hormones also play key roles in the development and progression of PCa [5].

Most PCa types are slow-growing and often asymptomatic, or their symptoms are similar to those of benign prostate hyperplasia (BPH) and are, hence, underestimated [6,7]. Since PCa is often asymptomatic in its earlier stages, it is very difficult to diagnose it before it reaches advanced stages. Late stages of PCa are associated with frequent night urination (nocturia), pain and difficulties during urination (dysuria), and the presence of blood in urine (haematuria) [8,9]. PCa may also cause problems with sexual function and performance [10].

PCa is screened via the analysis of the serological level of the prostate-specific antigen (PSA). Initially, the US Food and Drug Administration (FDA) agency approved PSA tests

together with a digital rectal examination (DRE) for PCa screening in 1994 [11]. A low level of PSA is present in healthy men, and an increased level is not only associated with PCa, but also with prostate enlargement, inflammation, and even cycling [7]. Hence, PSA is not a reliable PCa biomarker, with high false-negative and false-positive results due to the low specificity and sensitivity of the assay [7,8].

Since PSA is not able to provide reliable information as a biomarker for the diagnostics and screening of PCa, more specific biomarkers need to be studied and validated. Numerous types of biomolecules have been proposed as PCa biomarkers, including metabolites (i.e., sarcosine), proteins (i.e., prostate-specific antigen), RNAs (i.e., transmembrane protease serine 2-ETS-related gene fusion), and glycans [12–15].

Sarcosine is an intermediate metabolite involved in glycine synthesis and degradation. The first paper showing a link between changed sarcosine levels and cancer was published by A. Sreekumar and co-workers in 2009 [16]. Since this publication, there have been numerous studies that aimed to examine the association between sarcosine and PCa [17]. Elevated levels of sarcosine associated with prostate cancer can be found in prostate tissue, blood, and urine [18]. Significantly elevated levels of sarcosine are present in urine, and urine is the biofluid of choice since the analysis of biomarkers in urine is considered noninvasive [19].

The level of sarcosine in urine can vary from 20 nM to 5 μ M [20]. The role of sarcosine in the onset and development of the disease is the stimulation of the growth of malignant and metastatic cells [21]. Various methods are available for the determination of sarcosine [18,22–25] that exhibit several drawbacks that can be addressed with biosensing devices that are simple, fast, inexpensive, and reliable. Electrochemical techniques coupled with SPCEs can offer additional benefits to users, including portability and miniaturisation [26–28]. The integration of such devices for “cancer-on-a-chip” assay platforms is an additional advantage for their use in many applied areas [29,30].

We have been witnessing a revolution in the integration of nanomaterials to design biosensors over the past few decades. MXenes, discovered in 2011, are one of the largest families of two-dimensional (2D) materials for a diverse range of applications, including biosensing due to their high electrical conductivity, large active area, hydrophilic nature, easily tuneable structure, excellent thermal stability, and large interlayer spacing [31–34].

In this work, MXene $\text{Ti}_3\text{C}_2\text{T}_x$ was applied to the integration of sarcosine oxidase (SOx) onto SPCEs to fabricate a miniaturised, portable, cost-effective nanobiosensor for the ultrasensitive analysis of sarcosine as a PCa biomarker (Figure 1).

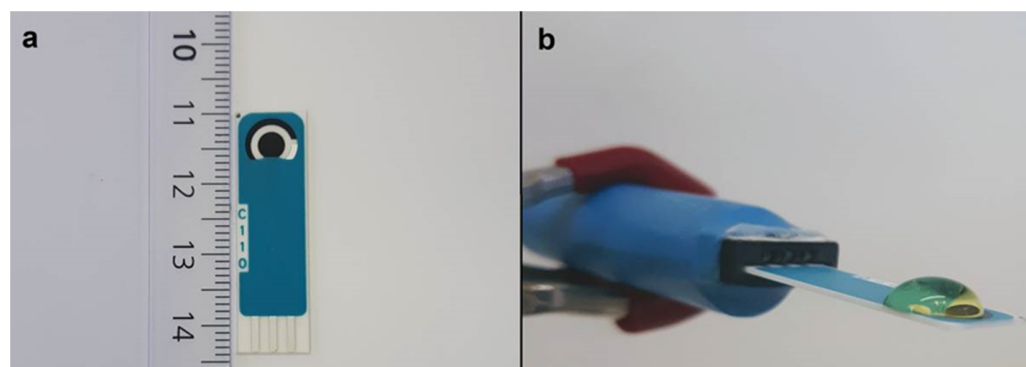


Figure 1. (a) Image of the SPCE electrode used to prepare the SOx/MXene–chitosan/SPCE biosensor. (b) Image of SOx/MXene–chitosan/SPCE electrode taken during CV analysis performed in 100 μ L droplet in the potential window from +0.1 V to -1.3 V vs. silver RE at a scan rate of $0.1 \text{ V}\cdot\text{s}^{-1}$ using 10 (blank) or 3 (sarcosine) scans.

The Materials and Methods section is provided in the supporting information file.

2. Results

2.1. Basic CV Studies in a Plain Buffer

Initial electrochemical experiments were performed by running CVs in a plain 0.1 M PB pH 7.4 in potential windows from 0.1 to -1.0 V (a cathodic window) and from 0.0 to 1.0 V (an anodic window) with a scan rate of $0.1 \text{ V}\cdot\text{s}^{-1}$ using modified SPCEs. The following electrodes were examined: SPCE, MXene/SPCE, MXene–chitosan/SPCE, and SOx/MXene–chitosan/SPCE (Figure 2).

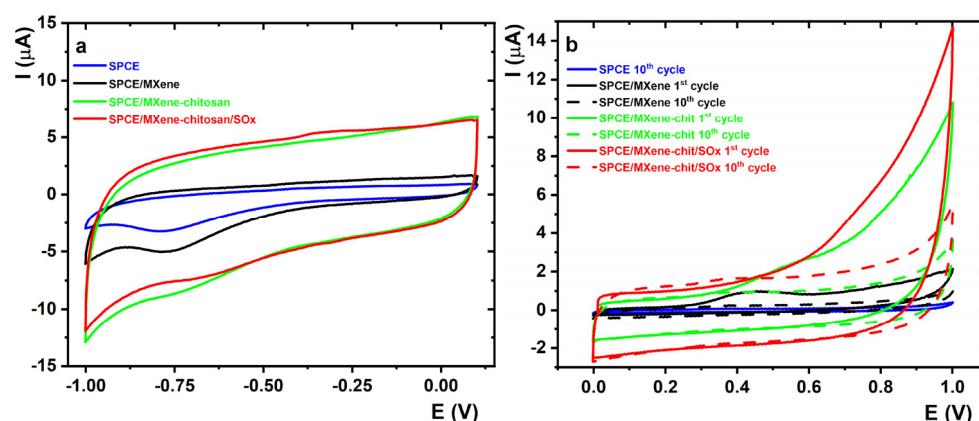


Figure 2. CVs in the plain 0.1 M PB pH 7.4 in (a) cathodic and (b) anodic potential windows with a scan rate of $100 \text{ mV}\cdot\text{s}^{-1}$ recorded using SPCE, MXene/SPCE, and MXene–chitosan/SPCE; SOx/MXene–chitosan/SPCE.

As shown in the Figure 2a, the capacitive current increased in the following order: unmodified SPCE, MXene/SPCE, MXene–chitosan/SPCE, and SOx/MXene–chitosan/SPCE. For MXene-modified SPCE, a higher current was observed than that of pristine SPCE because MXene/SPCE, due to the porous MXene structure, has a greater electrochemically active surface area when compared to the unmodified surface. These findings are in good agreement with already published results [35]. In the cases of MXene–chitosan/SPCE and SOx/MXene–chitosan/SPCE, the capacitive current was significantly higher than the unmodified SPCE and MXene/SPCE surface, suggesting the presence of enhanced MXene loading onto the electrode surface when present within the nanocomposite compared to the electrode modified only by MXene.

On the other hand, cyclic voltammetry in an anodic potential window (0.0 to 1.0 V) revealed that the MXene present on the MXene/SPCE surface underwent irreversible anodic oxidation with an oxidation peak at 0.457 V recorded in the first CV scan ($9.67 \pm 0.27 \times 10^{-7} \text{ A}$) (Figure 2b). The experiment revealed that the beneficial redox behaviour of MXene substantially dropped in the second scan, and a further decrease in anodic current with the increasing number of scans was observed. The exposure of MXene to an anodic potential in the aqueous solution oxidised the nanomaterial, forming a TiO_2 layer or TiO_2 domains with the subsequent TiO_2 dissolution by F^- ions, rendering the resulting nanomaterial less electrochemically active compared to the pristine MXene [36]. Similar results could be observed in the cases of the MXene–chitosan/SPCE and SOx/MXene–chitosan/SPCE surfaces. The prepared devices could, thus, be applied to electrochemical reactions in a cathodic potential window.

2.2. EIS Measurements Using a Ferricyanide/Ferrocyanide Redox Couple

EIS is a powerful characterisation technique to probe the interfacial properties of individual unmodified and modified SPCEs. EIS measurements were performed to observe the characteristics of individual modified SPCEs, and investigate the short-term stability of the prepared MXene/SPCE and MXene–chitosan/SPCE surfaces. Figure 3 shows the impedance spectra of the prepared modified electrodes.

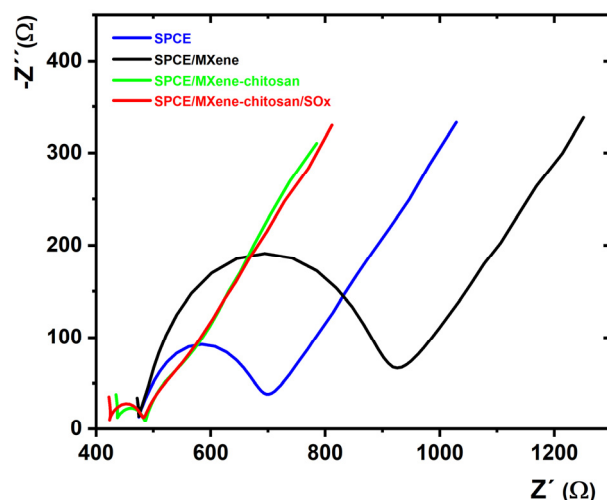


Figure 3. Nyquist plots of SPCE, MXene/SPCE, MXene–chitosan/SPCE, and SO_x/MXene–chitosan/SPCE in 0.1 M PB containing 5 mM K₃[Fe(CN)₆] and K₄[Fe(CN)₆]·3H₂O. Results are presented in the form of a Nyquist plot with equivalent circuit R[Q(RW)] applied for data fitting.

A Nyquist plot shows two main features: a semicircular part with a diameter representing charge transfer resistance R_{ct} and a linear part representing the diffusional properties of the interface [37].

EIS using a ferricyanide/ferrocyanide redox couple revealed that the R_{ct} of MXene-modified SPCE was approximately 1.9 times larger than that of bare SPCE (Table 1), indicating that a layer of negatively charged nanomaterial had formed on the surface, which hindered the electron transfer between $[\text{Fe}(\text{CN})_6]^{3-/4-}$ and the electrode surface (Table 1). Though MXene could hinder the electron transfer of a negatively charged soluble redox probe pair, it is an excellent candidate with high metallic conductivity and great film-forming ability for the design of electrochemical biosensors. In contrast, the MXene–chitosan/SPCE and SO_x/MXene–chitosan/SPCE surfaces exhibited significantly lower R_{ct} compared to those of the unmodified and MXene/SPCE. The R_{ct} value changed because of the electrostatic interactions between the positively charged chitosan-containing surface and $[\text{Fe}(\text{CN})_6]^{3-/4-}$ ions.

Table 1. R_{ct} values for each electrode modification obtained by running EIS in 0.1 M PB containing 5 mM K₃[Fe(CN)₆] and K₄[Fe(CN)₆]·3H₂O at 50 different frequencies in the range from 0.1 Hz to 100 kHz.

SPCE Modification	Charge Transfer Resistance (R_{ct}) Values (Ω)
SPCE	233 ± 4
MXene/SPCE	447 ± 10
MXene–chitosan/SPCE	52 ± 8
SO _x /MXene–chitosan/SPCE	66 ± 1

MXenes are promising nanoplatforms for the construction of biosensing devices due to their excellent physicochemical properties. A natural biopolymer, chitosan, is an excellent counterpart to MXene since it is a hydrophilic hydrogel that can form adhesive membranes/films with biocompatible properties [38,39]. Thus, the combination of chitosan and nanomaterials such as MXene is an efficient strategy for the design of mechanically robust biosensing devices [40,41].

In order to investigate the short-term stability of the prepared MXene/SPCE and MXene–chitosan/SPCE surfaces, and the stabilisation of nanomaterial with a chitosan matrix, seven subsequent EIS measurements were run in 0.1 M PB containing 5 mM K₃[Fe(CN)₆] and K₄[Fe(CN)₆]·3H₂O at 50 different frequencies in the range from 0.1 Hz

to 100 kHz. The obtained Nyquist plots of MXene/SPCE and MXene–chitosan/SPCE are presented in Figure 4.

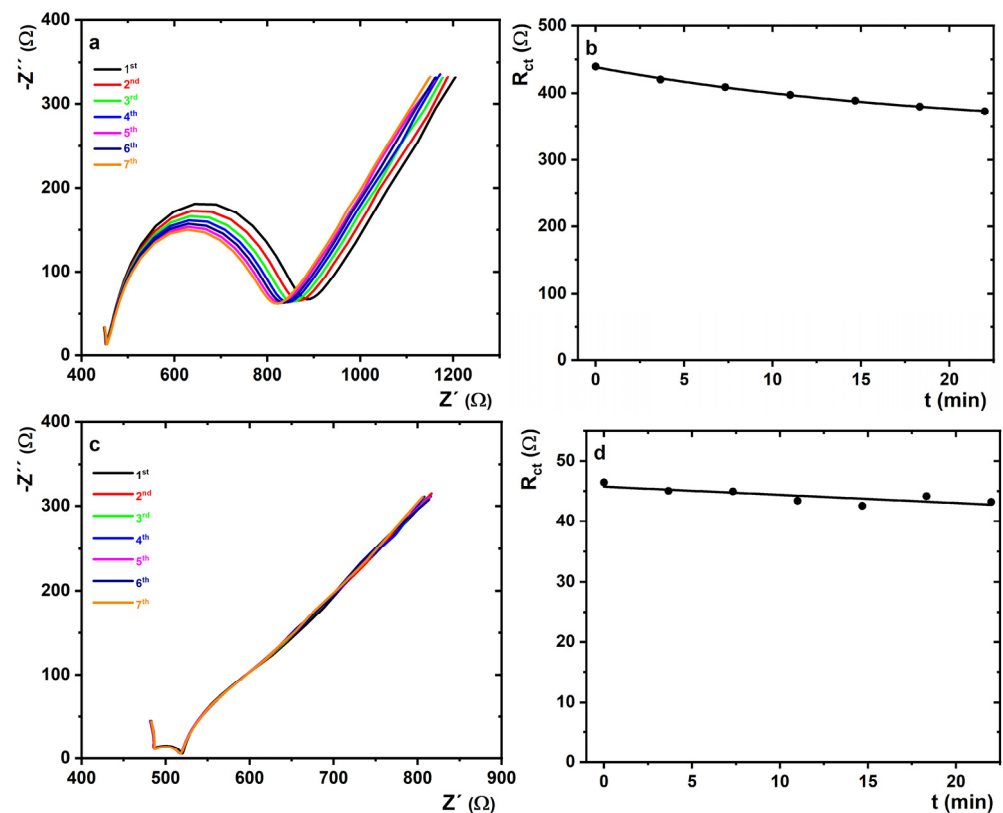


Figure 4. Nyquist plots of (a,b) MXene/SPCE and (c,d) MXene–chitosan/SPCE in 0.1 M PB pH 7.4 containing 5 mM $K_3[Fe(CN)_6]$ and $K_4[Fe(CN)_6] \cdot 3H_2O$ with measurements repeated 7 times. Results are presented in the form of a Nyquist plot, with an equivalent circuit $R[Q(RW)]$ applied for data fitting. The duration of the 7 subsequent EIS analyses was approximately 22 min.

The obtained results confirmed the stabilisation effect of the chitosan matrix on biosensor performance. In the case of the MXene/SPCE surface, a more significant change in R_{ct} value was observed compared to that on the MXene–chitosan/SPCE surface. The greatest decrease in R_{ct} value was recorded during the first four EIS measurements (Figure 4a). When the assay was performed in an electrochemical cell, a much quicker change (decrease) in R_{ct} was observed, i.e., 84.5% of the initial value on the MXene/SPCE interface (Figure 4b) compared to the assay performed on MXene–chitosan/SPCE (Figure 4c), i.e., 93.0% of the initial value (Figure 4d) within 22 min, indicating that chitosan had a positive effect on the stability of the MXene-modified interface. The exponential fitting of the operational stability curve performed on an electrochemical cell revealed that the signal would be stable at the R_{ct} value of 341 Ω (i.e., 77.6% of the initial value).

2.3. Detection of Sarcosine Using SOx/MXene–Chitosan/SPCE Biosensor

CV measurements with SOx/MXene–chitosan/SPCE electrodes for detection of sarcosine were performed in a cathodic potential window. SOx enzyme was characterised by maximal stability at pH value of 7.4 [42]. The bioelectrochemical activity of the biosensor was evaluated by constructing the corresponding calibration curves when 10 mM sarcosine stock solution was added into the cell during the measurement. The final sarcosine concentration was in the range of 2.5–50 μ M. Well-defined irreversible redox peaks were observed on the SOx/MXene–chitosan/SPCE electrode in the presence of sarcosine. The cathodic peak of H_2O_2 reduction increased with increasing biomarker concentration (Figure 5, inset). The plot of the peak current in the first CV scan vs. sarcosine concentration was applied to

calibrate the device by subtracting a blank signal. In this work, blank was considered the fifth CV scan obtained in the absence of sarcosine (Figure 5).

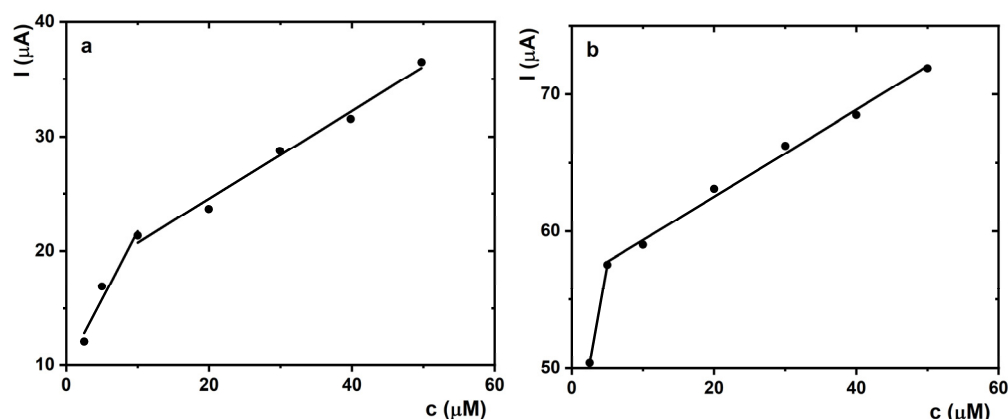


Figure 5. Calibration curves of the SO_x/MXene–chitosan/SPCE biosensor vs. sarcosine concentration. Inset: CVs of the prepared SO_x/MXene–chitosan/SPCE biosensor in 0.1 M PB pH 7.4 containing 0, 2.5, 5, 10, 20, 30, 40, 50 μM sarcosine at a scan rate of $0.1 \text{ V}\cdot\text{s}^{-1}$ in a potential window from +0.1 V to $-1.0/-1.3$ V. Measurements were run in the electrochemical cell by dipping SPCEs into (a) the solution or in (b) 100 μL of an electrolyte. CVs are shown in the Supplemental Figures S1 and S2, respectively.

In comparison with our previous study, several differences could be observed when working with SO_x/MXene–chitosan/SPCE biosensor compared to SO_x/MXene–chitosan/GCE device [43]. Significant differences in the values of the current responses were recorded. In the case of SPCE-based detection platform, they were about 19 times higher ($1.21 \times 10^{-5} \text{ A}$ in the presence of 2.5 μM sarcosine) in comparison with those of GCE-based biosensing ($6.38 \times 10^{-7} \text{ A}$ in the presence of 2.5 μM sarcosine). Changes in the current responses could be attributed to the properties of the carbon working-electrode material. The fitting of the calibration curve revealed two different ranges in which the calibration curve was linear for both types of measurements (Figure 5).

The assay in the electrochemical cell exhibited a first linear calibration curve in a range up to 10 μM with a slope of $1.19 \pm 0.25 \mu\text{A}\cdot\mu\text{M}^{-1}$ ($R^2 = 0.910$), and a second linear calibration curve in the range of 10–50 μM with a slope of $0.38 \pm 0.03 \mu\text{A}\cdot\mu\text{M}^{-1}$ ($R^2 = 0.982$) (Figure 5a). Additionally, the prepared SO_x/MXene–chitosan/SPCE biosensor exhibited a satisfactory LOD value of 7.0 nM. Hence, the LOD was successfully reduced by 2.6 times [43]. In comparison with the SO_x/MXene–chitosan/GCE device, a noticeable shift in peak potential values with respect to Ag/AgCl/KCl (3 M) RE was recorded. The peak potential shifted to more positive values with the increasing concentration of sarcosine. The electrochemical reduction in H₂O₂ by the device started at -0.2 V , with the peak maximum present at approx. -0.6 V (Figure 5, inset).

The proposed biosensing detection platform was subsequently further optimised. For this purpose, electrochemical measurements focusing on sample volume reduction were performed. For each measurement, drops with a volume of 100 μL were applied onto the surface of the SPCE's working electrode, since SPCEs are suitable for either working with microvolumes or dipping them into solutions. In this case, the electrochemical cell consisted of a modified carbon working electrode, carbon auxiliary electrode, and silver RE (Figure 5b). The assay run in 100 μL of an electrolyte showed a first linear calibration curve in the concentration window up to 5 μM with a slope of $2.86 \mu\text{A}\cdot\mu\text{M}^{-1}$ and a second linear calibration curve in the range of 5–50 μM with a slope of $0.32 \pm 0.01 \mu\text{A}\cdot\mu\text{M}^{-1}$ ($R^2 = 0.992$) (Figure 5b). In comparison with the previous measurement (Figure 5a), a shift in the reduction process towards more negative potentials was observed. The electrochemical reduction in H₂O₂ started at -0.5 V with the peak maximum present at -0.9 V . Such an electrochemical behaviour can be assigned to the characteristics

of the silver reference electrode used in three-electrode system. Moreover, similar findings were observed in the peak potential shift towards more positive values with an increasing concentration of sarcosine when compared to that in Figure 5a. Additionally, the prepared SOx/MXene–chitosan/SPCE biosensor exhibited a satisfactory LOD value of 10.4 nM. A slight increase in the LOD value in the case of the detection of sarcosine in the drop using the SOx/MXene–chitosan/SPCE device was caused by the increased intensity of noise during the electrochemical measurements. The intensified noise could be attributed to the nature of the used SPCE devices.

The reproducibility of the biosensor device’s fabrication, examined as the sensitivity of the devices, was within 10 % ($n = 5$) when measured in an electrochemical cell, and within 3 % ($n = 4$) when measured in 100 μ L of an electrolyte. Such observations indicate that it is much better to use the biosensor device for measurements in 100 μ L of an electrolyte with the bionanocomposite at the bottom in the measurement setup. Part of the bionanocomposite in the electrochemical cell was most likely dissolving over time.

The above MXene-based sarcosine biosensor device based on SPCEs is among the most sensitive applied to the analysis of sarcosine when comparing the LOD with that of other publications focused on the design of sarcosine sensors or biosensors (Table 2). Additionally, the as-fabricated biosensor belongs to the most sensitive MXene-based devices published so far when considering LOD (Table 3).

Table 2. Basic operational parameters of various (bio)sensors for the detection of sarcosine.

Detection	Surface Modification	LOD (nM)	Linear Range (μ M)	RT (s)	Stability	Application	Ref.
Amperometric	PVA–Ag/AuNPs–pphTEOS–SOx/GCE	500	0.5–7.5	17	NR	Aqueous media	[44]
Amperometric	SOx/EDC/NHS/Au/ZnONPs/SPEs	16	0.01–0.1	NR	60 days	Synthetic urine	[45]
Amperometric	SOx/CHIT/CuNPs/cMWCNT/AuE	0.0001	0.1–100	2	180 days	Human serum	[46]
Amperometric	SOxNPs/AuE	10	0.1–100	2	180	Urine	[47]
Amperometric	SOx/Pt@ZIF8/GCE	1060	5–30	NR	3	Urine	[48]
Amperometric	Nafion–SOx/Pt/AAO	50	0.05–100	NR	NR	Aqueous media	[20]
Amperometric	SOx/Pt/OIHMP/GCE	130	1–70	NR	NR	Human serum	[49]
Amperometric	SOx/PAA/GCE	0.4	0.001–0.05	NR	15 days	Urine	[50]
Amperometric	SOx/Pt–Fe ₃ O ₄ @C/GCE	430	0.5–60	NR	NR	Human serum	[51]
Amperometric	Fe ₃ O ₄ @ZIF–8@MIP/AuE	0.0004	0.000001–0.0001	NR	NR	Urine	[52]
Amperometric	SOx/chitosan/Ti ₃ C ₂ T _x /GCE	18	0.036–7.8	2	NR	Synthetic urine	[43]
Amperometric	SOx/chitosan/Ti ₃ C ₂ T _x /SPE	7	0.1–1.0	NR	NR	Synthetic urine	this work
Potentiometric	MIP-based sensor	0.14	0.001–10	<120	>5 months	Aqueous media	[53]
Potentiometric	Antisarcosine–Ab–GFOX@graphite–powder@dibutyl phthalate–electrode	0.003	0.01–100	60	3–4 months	Aqueous media	[54]
Potentiometric	Antisarcosine–Ab@graphite–powder@dibutyl phthalate–electrode	0.005	0.001–10	60	3–4 months	Aqueous media	[54]
Impedimetric	MIP/AuNPs/SPCE	8.5	0.011–17.9	NR	~7 days	Aqueous media	[55]
Colorimetric	PdNP-based sensing platform	5.0	0.01–50	NR	NR	Urine	[56]

Table 2. Cont.

Detection	Surface Modification	LOD (nM)	Linear Range (µM)	RT (s)	Stability	Application	Ref.
Colorimetric	NQS/GO/GCE	730	6.2–26.3	NR	NR	Aqueous media	[57]
Fluorimetric	Nanomagemite/AuNPs/QD/peptide	0.05	0.005–0.05	NR	NR	Urine Cell lines	[58]
Fluorimetric	ssDNA aptamer-based sensor	55	0.1–2	NR	NR	Urine	[59]

Abbreviations: LOD—limit of detection, RT—response time, PVA—polyvinyl alcohol, pph-TEOS—partially prehydrolysed tetraethyl orthosilicate, CHIT—chitosan, cMWCNT—carboxylated multi-walled carbon nanotubes, Pt@ZIF8—nanoplatinum-loaded porous zeolitic imidazolate framework-8, AAO—ano-dised aluminium oxide, Pt/OIHMP—platinum-supported mesoporous organic-inorganic hybrid molybdenum phosphate, MIP—molecularly imprinted polymer, GO—graphene oxide, GO-based nanocomposite: Ab-GO@graphite-powder@dibutyl phthalate-electrode; NQS—1,2-naphthoquinone-4-sulphonic acid sodium salt, NR—not reported.

Table 3. Operational performance of electrochemical MXene-based (bio)sensors.

Analyte	Detection	LOD	Linear range	Reference
Glucose	Amperometry	5.9 µM	0.1–18 mM	[60]
H ₂ O ₂	Amperometry	0.02 µM	0.1–260 µM	[61]
NO ₂ ⁻	Amperometry	0.12 µM	0.5 µM–11.8 mM	[35]
H ₂ O ₂	Amperometry	14.0 nM	0.1–380 µM	[62]
H ₂ O ₂	Voltammetry (DPV)	1.95 µM	2 µM–1 mM	[63]
H ₂ O ₂	Amperometry	448 nM	490 µM–53.6 mM	[64]
AA, DA, UA, APAP	Voltammetry (DPV)	0.25 µM, 0.26 µM, 0.12 µM, 0.13 µM	Up to 750 µM	[64]
H ₂ O ₂	Chronoamperometry	0.7 nM	NR	[36]
DA	FET	100 × 10 ⁻⁹ M	100 × 10 ⁻⁹ –50 × 10 ⁻⁶ M	[65]
P53 gene	ECL	5 nM	10 nM–1 mM	[66]
Phenol	Amperometry	12 nM	0.05–15.5 µM	[67]
Cd ²⁺ , Pb ²⁺ , Cu ²⁺ , Hg ²⁺	Voltammetry (SWASV)	98 nM, 41 nM, 32 nM, 130 nM	0.1–1.5 µM	[68]
BrO ₃ ⁻	Voltammetry	41 nM	50 nM–5 µM	[69]
Malathion	Voltammetry (DPV)	0.3 × 10 ⁻¹⁴ M	1 × 10 ⁻¹⁴ –1 × 10 ⁻⁸ M	[70]
Sarcosine	Chronoamperometry	18 nM	36 nM–7.8 µM	[43]
Sarcosine	Cyclic voltammetry (CV)	7 nM	0.1–1.0 µM	This work

Abbreviations: AA—ascorbic acid, APAP—acetaminophen, DA—dopamine, DPV—differential pulse voltammetry, ECL—electrochemiluminescence, FET—field effect transistor, SWASV—square-wave stripping voltammetry, UA—uric acid [71].

Scanning electron microscopy was used to visualise both pristine MXene (Figure 6, left) and the Ti₃C₂T_x MXene@chitosan composite (Figure 6, right).

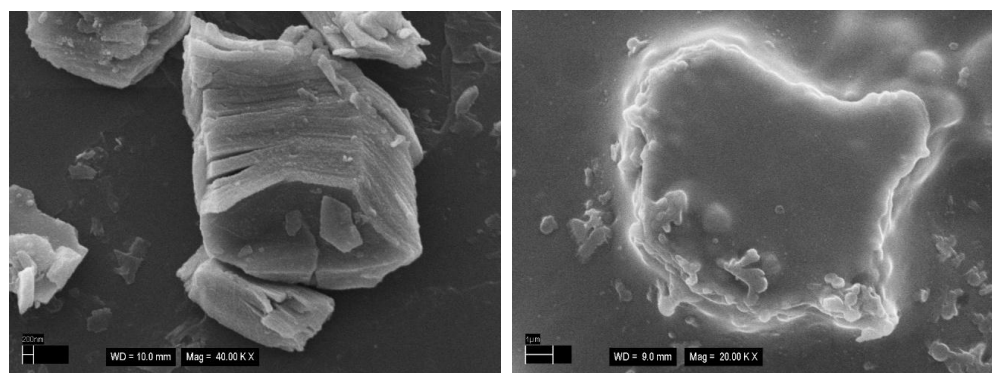


Figure 6. Scanning electron microscopy images representing (left) pristine multilayered $\text{Ti}_3\text{C}_2\text{T}_x$ MXene structure, 40,000 \times and (right) $\text{Ti}_3\text{C}_2\text{T}_x$ MXene@chitosan composite, 20,000 \times .

2.4. Clinical Application of SO_x/MXene –Chitosan/SPCE Biosensor

The practical application of the biosensor was evaluated by analysing the analyte in real samples. For that purpose, the SO_x/MXene –chitosan/SPCE device was applied to analyse sarcosine (from 0.1 to 1.0 μM) spiked into 10 \times diluted artificial urine using sarcosine as the PCa biomarker [20]. Calibration curves were obtained from measurements in 0.1 M PB pH 7.4 and 10 \times diluted artificial urine together with the CVs of the prepared SO_x/MXene –chitosan/SPCE biosensor. The value of the obtained recovery index was 92.5% (data not shown). The recovery index was calculated via the standard addition of 1 μM sarcosine into artificial urine, and the current response obtained in urine was compared to the current response obtained in plain PB. This means that, under such conditions, there were no significant interferences affecting the biosensor's performance. The results prove that the as-fabricated biosensor is a reliable tool for sarcosine detection in urine samples. Obviously, analysis with real human urine is needed to reach more general conclusions about the performance of the prepared MXene-based sarcosine biosensor in the analysis of real urine samples.

2.5. Long-Term Stability of the SO_x/MXene –Chitosan/SPCE Device

To investigate the long-term stability of the prepared SO_x/MXene –chitosan/SPCE device, CV measurements in the presence of 30 μM sarcosine in the potential window from 0.1 to -1.0 V and 0.1 to -1.3 V in the cell and in a 100 μL droplet, respectively, were performed (Figure 7). All prepared devices were stored in the refrigerator throughout the experiment.

In the case of the performed measurements in the cell (Figure 7a), the average current responses of the prepared SO_x/MXene –chitosan/SPCE device decreased from $7.05 \pm 0.51 \times 10^{-5}$ A on day 0 to $5.94 \pm 0.65 \times 10^{-5}$ A on Day 35 after biosensor preparation. Thus, a 15.7% drop of the SO_x/MXene –chitosan/SPCE current response was observed for measurements in the cell within 35 days. For the measurements performed in the 100 μL droplet (Figure 7b), a 6.8% decrease in the SO_x/MXene –chitosan/SPCE current response was observed on Day 35 after fabrication. In this case, the average current responses of the prepared SO_x/MXene –chitosan/SPCE device decreased from $6.12 \pm 0.77 \times 10^{-5}$ A on Day 0 to $5.71 \pm 0.01 \times 10^{-5}$ A on Day 35. Despite a slight decrease in the current response, the as-fabricated SO_x/MXene –chitosan/SPCE device was able to detect sarcosine even after a period of 5 weeks. In summary, the obtained data confirm that the as-fabricated device could be used for analysis for at least 5 weeks after its preparation.

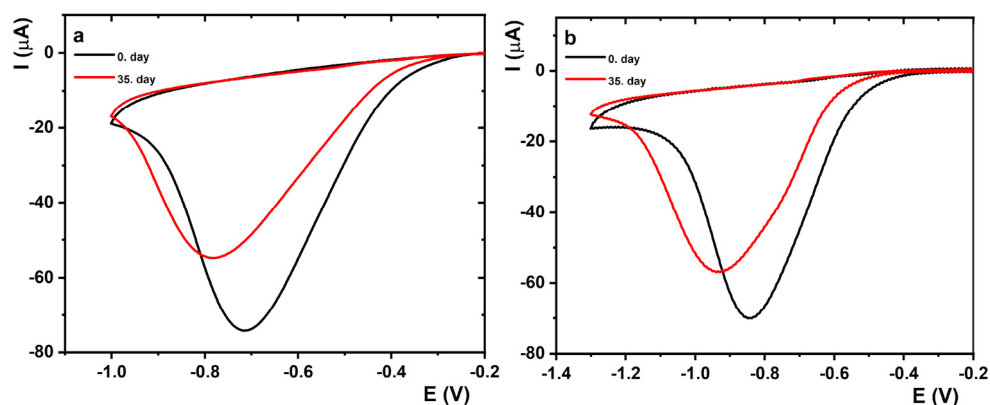


Figure 7. (a) CVs after the subtraction of the blank of the prepared SOx/MXene–chitosan/SPCE biosensor in 0.1 M PB pH 7.4 in a cell containing 30 μM sarcosine at a scan rate of $0.1 \text{ V}\cdot\text{s}^{-1}$ in a potential window from 0.1 to -1.0 V measured on days 0 (black) and 35 (red) after its preparation. (b) CVs after the subtraction of the blank of the SOx/MXene–chitosan/SPCE biosensor in 0.1 M PB pH 7.4 containing 30 μM sarcosine at a scan rate of $0.1 \text{ V}\cdot\text{s}^{-1}$ in a potential window from 0.1 to -1.3 V measured on days 0 (black) and 35 (red) after preparation. During each measurement, 100 μL was applied to the surface of SPCE electrode.

3. Conclusions

The goal of this paper was to design an enzymatic nanobiosensor for the detection of PCa biomarkers using disposable SPCEs and modern 2D nanomaterial MXene in order to prepare a sensitive, reliable, portable and miniaturised, stable, cost-effective, and quick detection platform based on previously obtained results and findings. By dipping SPCEs into the solution, the prepared SOx/MXene–chitosan/SPCE biosensor exhibited a satisfactory LOD value of 7.0 nM. Hence, the LOD was successfully reduced 2.6 times when compared to our previous paper. The proposed detection platform was subsequently further optimised with a focus on a sample volume reduction of up to 100 μL , exhibiting a satisfactory LOD value of 10.4 nM. To investigate the long-term stability of the prepared SOx/MXene–chitosan/SPCE device, CV measurements were performed in the presence of 30 μM in both the cell and a 100 μL droplet. For the measurements performed in the 100 μL droplet, only a 6.8% decrease in the SOx/MXene–chitosan/SPCE current response could be observed during the first 35 days after fabrication. Thus, the obtained data confirm that the as-fabricated device could be used for the detection of sarcosine in urine for a period of at least 5 weeks after its preparation. Moreover, to evaluate the potential application of the biosensor for the analysis of real samples, the as-fabricated device was successfully applied for the determination of sarcosine spiked into $10\times$ diluted artificial urine with the 92.5% recovery index value. Such results prove that the as-fabricated biosensor is a reliable tool for sarcosine detection in urine samples. The portable SOx/MXene–chitosan/SPCE device is one of the most sensitive electrochemical biosensor devices for the analysis of sarcosine when classified by LOD. Additionally, the as-fabricated MXene-based biosensor is one of the most sensitive MXene-based devices.

Supplementary Materials: The following supporting information can be downloaded at: <https://www.mdpi.com/article/10.3390/jfb14030161/s1>, Figure S1: Enlarged graph shown in Figure 5A in the inset; Figure S2: Enlarged graph shown in Figure 5B in the inset.

Author Contributions: Conceptualisation, T.B. and J.T.; methodology, L.L., T.B., M.B., P.K. and J.T.; validation, S.H. and L.L.; formal analysis, M.H. and E.J.; investigation, S.H., L.L., M.H. and E.J.; resources, M.B., P.K. and J.T.; data curation, S.H., L.L. and J.T.; writing—original draft preparation, S.H., L.L. and J.T.; writing—review and editing, S.H., L.L., T.B., M.H., E.J., M.B., P.K. and J.T.; supervision, T.B. and M.B.; project administration, M.B., P.K. and J.T.; funding acquisition, M.B., P.K. and J.T. All authors have read and agreed to the published version of the manuscript.

Funding: This research was funded by the Slovak Research and Development Agency (APVV-20-0272 and APPV 17-0300) and by the Slovak Scientific Grant Agency (VEGA 2/0137/18 and 2/0130/20). We would like to acknowledge the support received from the Ministry of Health of the Slovak Republic under project registration number 2019/68-CHÚSAV-1. This publication was created with the support of the Operational Programme Integrated Infrastructure for the project of Center for Biomedical Research-BIOMEDIRES-II stage (ITMS: 313011W428) co-financed by the European Regional Development Fund. P.K. thanks that this publication was jointly supported by Qatar University grant # QUCCG-CAM-22/23-504.

Data Availability Statement: Research data are available upon request.

Conflicts of Interest: The authors declare no conflict of interest.

References

- Sung, H.; Ferlay, J.; Siegel, R.L.; Laversanne, M.; Soerjomataram, I.; Jemal, A.; Bray, F. Global Cancer Statistics 2020: GLOBOCAN Estimates of Incidence and Mortality Worldwide for 36 Cancers in 185 Countries. *Cancer J. Clin.* **2021**, *71*, 209–249. [[CrossRef](#)]
- Nuhić, J.; Kevrić, J. Prostate Cancer Detection Using Different Classification Techniques. In *CMBEBIH 2019*; Springer: Banja Luka, Bosnia and Herzegovina, 2020; pp. 67–73.
- Rawla, P. Epidemiology of Prostate Cancer. *World J. Oncol.* **2019**, *10*, 63–89. [[CrossRef](#)]
- Bertok, T.; Bertokova, A.; Hroncekova, S.; Chocholova, E.; Svecova, N.; Lorencova, L.; Kasak, P.; Tkac, J. Novel Prostate Cancer Biomarkers: Aetiology, Clinical Performance and Sensing Applications. *Chemosensors* **2021**, *9*, 205. [[CrossRef](#)]
- Bostwick, D.G.; Burke, H.B.; Djakiew, D.; Euling, S.; Ho, S.M.; Landolph, J.; Morrison, H.; Sonawane, B.; Shifflett, T.; Waters, D.J.; et al. Human prostate cancer risk factors. *Cancer* **2004**, *101*, 2371–2490. [[CrossRef](#)]
- Tkac, J.; Bertok, T.; Hires, M.; Jane, E.; Lorencova, L.; Kasak, P. Glycomics of prostate cancer: Updates. *Exp. Rev. Proteom.* **2019**, *16*, 65–76. [[CrossRef](#)]
- Tkac, J.; Gajdosova, V.; Hroncekova, S.; Bertok, T.; Hires, M.; Jane, E.; Lorencova, L.; Kasak, P. Prostate-specific antigen glycoprofiling as diagnostic and prognostic biomarker of prostate cancer. *Interface Focus* **2019**, *9*, 20180077. [[CrossRef](#)]
- Damborsky, P.; Damborska, D.; Belicky, S.; Tkac, J.; Katrlík, J. Sweet Strategies in Prostate Cancer Biomarker Research: Focus on a Prostate Specific Antigen. *BioNanoScience* **2017**, *8*, 690–700. [[CrossRef](#)]
- Talcott, A.; Rieker, P.; Clark, J.A.; Probert, K.J.; Weeks, J.C.; Beard, C.J.; Wishnow, K.I.; Kaplan, I.; Laughlin, K.R.; Richie, J.P.; et al. Patient-Reported Symptoms After Primary Therapy for Early Prostate Cancer: Results of a Prospective Cohort Study. *J. Clin. Oncol.* **1998**, *16*, 275–283. [[CrossRef](#)]
- Miller, D.C.; Hafez, K.S.; Stewart, A.; Montie, J.E.; Wei, J.T. Prostate carcinoma presentation, diagnosis, and staging: An update from the National Cancer Data Base. *Cancer* **2003**, *98*, 1169–1178. [[CrossRef](#)]
- O'Reilly, J.; O'Kennedy, R.J. Prostate Cancer Detection: Complexities and Strategies. *J. Cancer Treat. Diagn.* **2017**, *2*, 18–25. [[CrossRef](#)]
- Katafigioti, A.; Katafigiotis, I.; Sfoungaristos, S.; Alamanis, C.; Stravodimos, K.; Anastasiou, I.; Roumelioti, E.; Duvdevani, M.; Constantinides, C. In the search of novel urine biomarkers for the early diagnosis of prostate cancer. Intracellular or secreted proteins as the target group? Where and how to search for possible biomarkers useful in the everyday clinical practice. *Arch. Ital. Urol. Androl.* **2016**, *88*, 195–200. [[CrossRef](#)]
- Jakobsen, N.A.; Hamdy, F.C.; Bryant, R.J. Novel biomarkers for the detection of prostate cancer. *J. Clin. Urol.* **2016**, *9*, 3–10. [[CrossRef](#)]
- Bertok, T.; Lorencova, L.; Hroncekova, S.; Gajdosova, V.; Jane, E.; Hires, M.; Kasak, P.; Kaman, O.; Sokol, R.; Bella, V.; et al. Advanced impedimetric biosensor configuration and assay protocol for glycoprofiling of a prostate oncomarker using Au nanoshells with a magnetic core. *Biosens. Bioelectron.* **2019**, *131*, 24–29. [[CrossRef](#)]
- Bertokova, A.; Bertok, T.; Jane, E.; Hires, M.; Dubjakova, P.; Novotna, O.; Belan, V.; Fillo, J.; Tkac, J. Detection of N,N-diacetyllactosamine (LacdiNAc) containing free prostate-specific antigen for early stage prostate cancer diagnostics and for identification of castration-resistant prostate cancer patients. *Biorg. Med. Chem.* **2021**, *39*, 116156. [[CrossRef](#)]
- Sreekumar, A.; Poisson, L.M.; Rajendiran, T.M.; Khan, A.P.; Cao, Q.; Yu, J.; Laxman, B.; Mehra, R.; Lonigro, R.J.; Li, Y.; et al. Metabolomic profiles delineate potential role for sarcosine in prostate cancer progression. *Nature* **2009**, *457*, 910–914. [[CrossRef](#)]
- Yousefi, M.; Qujeq, D.; Shafi, H.; Tilaki, K.H. Serum and Urine Levels of Sarcosine in Benign Prostatic Hyperplasia and Newly Diagnosed Prostate Cancer Patients. *J. Kermanshah Univ. Med. Sci.* **2020**, *24*, e970002020. [[CrossRef](#)]
- Cernei, N.; Heger, Z.; Gumulec, J.; Zitka, O.; Masarik, M.; Babula, P.; Eckschlager, T.; Stiborova, M.; Kizek, R.; Adam, V. Sarcosine as a potential prostate cancer biomarker—a review. *Int. J. Mol. Sci.* **2013**, *14*, 13893–13908. [[CrossRef](#)]
- Jornet-Martínez, N.; Henderson, C.J.; Campíns-Falcó, P.; Daly, R.; Hall, E.A.H. Towards sarcosine determination in urine for prostatic carcinoma detection. *Sens. Actuat. B Chem.* **2019**, *287*, 380–389. [[CrossRef](#)]
- Hu, J.; Wei, W.; Ke, S.; Zeng, X.; Lin, P. A novel and sensitive sarcosine biosensor based on organic electrochemical transistor. *Electrochim. Acta* **2019**, *307*, 100–106. [[CrossRef](#)]
- Khan, A.P.; Rajendiran, T.M.; Ateeq, B.; Asangani, I.A.; Athanikar, J.N.; Yocum, A.K.; Mehra, R.; Siddiqui, J.; Palapattu, G.; Wei, J.T.; et al. The role of sarcosine metabolism in prostate cancer progression. *Neoplasia* **2013**, *15*, 491–501. [[CrossRef](#)]

22. Mazzu-Nascimento, T.; Gomes Carneiro Leão, P.A.; Catai, R.J.; Morbioli, G.; Carrilho, E. Towards low-cost bioanalytical tools for sarcosine assays for cancer diagnostics. *Anal. Methods* **2016**, *8*, 7312–7318. [[CrossRef](#)]
23. Burton, C.; Gamagedara, S.; Ma, Y. A novel enzymatic technique for determination of sarcosine in urine samples. *Anal. Methods* **2012**, *4*, 141–146. [[CrossRef](#)]
24. Cernei, N.; Zitka, O.; Ryvolova, M.; Adam, V.; Masarik, M.; Hubalek, J.; Kizek, R. Spectrometric and Electrochemical Analysis of Sarcosine as a Potential Prostate Carcinoma Marker. *Int. J. Electrochem. Sci.* **2012**, *7*, 4286–4301.
25. Jiang, Y.; Cheng, X.; Wang, C.; Ma, Y. Quantitative Determination of Sarcosine and Related Compounds in Urinary Samples by Liquid Chromatography with Tandem Mass Spectrometry. *Anal. Chem.* **2010**, *82*, 9022–9027. [[CrossRef](#)] [[PubMed](#)]
26. Torres-Rivero, K.; Florido, A.; Bastos-Arrieta, J. Recent Trends in the Improvement of the Electrochemical Response of Screen-Printed Electrodes by Their Modification with Shaped Metal Nanoparticles. *Sensors* **2021**, *21*, 2596. [[CrossRef](#)] [[PubMed](#)]
27. Suresh, R.R.; Lakshmanakumar, M.; Arockia Jayalatha, J.B.B.; Rajan, K.S.; Sethuraman, S.; Krishnan, U.M.; Rayappan, J.B.B. Fabrication of screen-printed electrodes: Opportunities and challenges. *J. Mater. Sci.* **2021**, *56*, 8951–9006. [[CrossRef](#)]
28. Yanez-Sedeno, P.; Campuzano, S.; Pingarron, J.M. Screen-Printed Electrodes: Promising Paper and Wearable Transducers for (Bio)Sensing. *Biosensors* **2020**, *10*, 76. [[CrossRef](#)] [[PubMed](#)]
29. Cui, F.; Zhou, Z.; Zhou, H.S. Review—Measurement and Analysis of Cancer Biomarkers Based on Electrochemical Biosensors. *J. Electrochem. Soc.* **2020**, *167*, 037525. [[CrossRef](#)]
30. García-Miranda Ferrari, A.; Rowley-Neale, S.J.; Banks, C.E. Screen-printed electrodes: Transitioning the laboratory in-to-the field. *Talanta Open* **2021**, *3*, 100032. [[CrossRef](#)]
31. Jun, B.M.; Kim, S.; Heo, J.; Park, C.M.; Her, N.; Jang, M.; Huang, Y.; Han, J.; Yoon, Y. Review of MXenes as new nanomaterials for energy storage/delivery and selected environmental applications. *Nano Res.* **2018**, *12*, 471–487. [[CrossRef](#)]
32. Hart, J.L.; Hantanasirisakul, K.; Lang, A.C.; Anasori, B.; Pinto, D.; Pivak, Y.; van Omme, J.T.; May, S.J.; Gogotsi, Y.; Taheri, M.L. Control of MXene's electronic properties through termination and intercalation. *Nat. Commun.* **2019**, *10*, 522. [[CrossRef](#)] [[PubMed](#)]
33. Anasori, B.; Lukatskaya, M.R.; Gogotsi, Y. 2D metal carbides and nitrides (MXenes) for energy storage. *Nat. Rev. Mat.* **2017**, *2*, 16098. [[CrossRef](#)]
34. Hong, W.; Wyatt, B.C.; Nemani, S.K.; Anasori, B. Double transition-metal MXenes: Atomistic design of two-dimensional carbides and nitrides. *MRS Bull.* **2020**, *45*, 850–861. [[CrossRef](#)]
35. Liu, H.; Duan, C.; Yang, C.; Shen, W.; Wang, F.; Zhu, Z. A novel nitrite biosensor based on the direct electrochemistry of hemoglobin immobilized on MXene-Ti₃C₂. *Sens. Actuat. B Chem.* **2015**, *218*, 60–66. [[CrossRef](#)]
36. Lorencova, L.; Bertok, T.; Dosekova, E.; Holazova, A.; Paprckova, D.; Vikartovska, A.; Sasinkova, V.; Filip, J.; Kasak, P.; Jerigova, M.; et al. Electrochemical performance of Ti₃C₂T_x MXene in aqueous media: Towards ultrasensitive H₂O₂ sensing. *Electrochim. Acta* **2017**, *235*, 471–479. [[CrossRef](#)]
37. Feng, J.J.; Zhao, G.; Xu, J.J.; Chen, H.Y. Direct electrochemistry and electrocatalysis of heme proteins immobilized on gold nanoparticles stabilized by chitosan. *Anal. Biochem.* **2005**, *342*, 280–286. [[CrossRef](#)]
38. Yang, P.; Gao, X.; Wang, L.; Wu, Q.; Chen, Z.; Lin, X. Amperometric sensor for ascorbic acid based on a glassy carbon electrode modified with gold-silver bimetallic nanotubes in a chitosan matrix. *Microchim. Acta* **2013**, *181*, 231–238. [[CrossRef](#)]
39. Suginta, W.; Khunkaewla, P.; Schulte, A. Electrochemical biosensor applications of polysaccharides chitin and chitosan. *Chem. Rev.* **2013**, *113*, 5458–5479. [[CrossRef](#)]
40. Hao, C.; Shen, Y.; Shen, J.; Xu, K.; Wang, X.; Zhao, Y.; Ge, C. A glassy carbon electrode modified with bismuth oxide nanoparticles and chitosan as a sensor for Pb(II) and Cd(II). *Microchim. Acta* **2016**, *183*, 1823–1830. [[CrossRef](#)]
41. Xu, W.; Qing, Y.; Chen, S.; Chen, J.; Qin, Z.; Qiu, J.; Li, C. Electrochemical indirect competitive immunoassay for ultrasensitive detection of zearalenone based on a glassy carbon electrode modified with carboxylated multi-walled carbon nanotubes and chitosan. *Microchim. Acta* **2017**, *184*, 3339–3347. [[CrossRef](#)]
42. Matsuda, Y.; Hoshika, H.; Inouye, Y.; Ikuta, S.; Matsuura, K.; Nakamura, S. Purification and Characterization of Sarcosine oxidase of *Bacillus* Origin. *Chem. Pharm. Bull.* **1987**, *35*, 711–717. [[CrossRef](#)] [[PubMed](#)]
43. Hroncekova, S.; Bertok, T.; Hires, M.; Jane, E.; Lorencova, L.; Vikartovska, A.; Tanvir, A.; Kasak, P.; Tkac, J. Ultrasensitive Ti₃C₂T_x MXene/chitosan nanocomposite-based amperometric biosensor for detection of potential prostate cancer marker in urine samples. *Processes* **2020**, *8*, 580. [[CrossRef](#)]
44. Lad, U.; Kale, G.M.; Bryaskova, R. Sarcosine Oxidase Encapsulated Polyvinyl Alcohol-Silica-AuNP Hybrid Films for Sarcosine Sensing Electrochemical Bioelectrode. *J. Electrochem. Soc.* **2014**, *161*, B98–B101. [[CrossRef](#)]
45. Rebelo, T.S.; Pereira, C.M.; Sales, M.G.; Norona, J.P.; Costa-Rodrigues, J.; Silva, F.; Fernandes, M.H. Sarcosine oxidase composite screen-printed electrode for sarcosine determination in biological samples. *Anal. Chim. Acta* **2014**, *850*, 26–32. [[CrossRef](#)]
46. Narwal, V.; Kumar, P.; Joon, P.; Pundir, C.S. Fabrication of an amperometric sarcosine biosensor based on sarcosine oxidase/chitosan/CuNPs/c-MWCNT/Au electrode for detection of prostate cancer. *Enzyme Microb. Technol.* **2018**, *113*, 44–51. [[CrossRef](#)]
47. Kumar, P.; Narwal, V.; Jaiwal, R.; Pundir, C.S. Construction and application of amperometric sarcosine biosensor based on SOxNPs/AuE for determination of prostate cancer. *Biosens. Bioelectron.* **2018**, *122*, 140–146. [[CrossRef](#)]
48. Yang, H.; Wang, J.; Yang, C.; Zhao, X.; Xie, S.; Ge, Z. Nano Pt@ZIF8 Modified Electrode and Its Application to Detect Sarcosine. *J. Electrochem. Soc.* **2018**, *165*, H247–H250. [[CrossRef](#)]

49. Wang, Q.; Zhao, Y.; Yang, Q.; Du, D.; Yang, H.; Lin, Y. Amperometric sarcosine biosensor with strong anti-interference capabilities based on mesoporous organic-inorganic hybrid materials. *Biosens. Bioelectron.* **2019**, *141*, 111431. [[CrossRef](#)]
50. Li, J.; Ma, J.; Zhang, Y.; Zhang, Z.; He, G. An amperometric biosensor for the assay of sarcosine based on the cross coupled chemical and electrochemical reactions with practical applications. *J. Electroanal. Chem.* **2019**, *833*, 568–572. [[CrossRef](#)]
51. Yang, Q.; Li, N.; Li, Q.; Chen, S.; Wang, H.; Yang, H. Amperometric sarcosine biosensor based on hollow magnetic Pt-Fe₃O₄@C nanospheres. *Anal. Chim. Acta* **2019**, *1078*, 161–167. [[CrossRef](#)] [[PubMed](#)]
52. Tang, P.; Wang, Y.; He, F. Electrochemical sensor based on super-magnetic metal-organic framework@molecularly imprinted polymer for Sarcosine detection in urine. *J. Saudi Chem. Soc.* **2020**, *24*, 620–630. [[CrossRef](#)]
53. Özkütük, E.B.; Diltemiz, S.E.; Avci, S.; Ugurag, D.; Aykanat, R.B.; Ersoz, A.; Say, R. Potentiometric sensor fabrication having 2D sarcosine memories and analytical features. *Mater. Sci. Eng. C* **2016**, *69*, 231–235. [[CrossRef](#)]
54. Altunkök, N.; Biçen Ünlüer, Ö.; Birlik Özkütük, E.; Ersöz, A. Development of potentiometric biosensor for diagnosis of prostate cancer. *Mater. Sci. Eng. B* **2021**, *263*, 114789. [[CrossRef](#)]
55. Nguy, T.P.; Van Phi, T.; Tram, D.T.N.; Eersels, K.; Wagner, P.; Lien, T.T.N. Development of an impedimetric sensor for the label-free detection of the amino acid sarcosine with molecularly imprinted polymer receptors. *Sens. Actuat. B Chem.* **2017**, *246*, 461–470. [[CrossRef](#)]
56. Lan, J.; Xu, W.; Wan, Q.; Zhang, X.; Lin, J.; Chen, J.; Chen, J. Colorimetric determination of sarcosine in urine samples of prostatic carcinoma by mimic enzyme palladium nanoparticles. *Anal. Chim. Acta* **2014**, *825*, 63–68. [[CrossRef](#)]
57. Xue, Z.; Yin, B.; Wang, H.; Li, M.; Rao, H.; Liu, X.; Zhou, X.; Lu, X. An organic indicator functionalized graphene oxide nanocomposite-based colorimetric assay for the detection of sarcosine. *Nanoscale* **2016**, *8*, 5488–5496. [[CrossRef](#)]
58. Heger, Z.; Cernei, N.; Krizkova, S.; Masarik, M.; Kopel, P.; Hodek, P.; Zitka, O.; Adam, V.; Kizek, R. Paramagnetic nanoparticles as a platform for FRET-based sarcosine picomolar detection. *Sci. Rep.* **2015**, *5*, 8868. [[CrossRef](#)] [[PubMed](#)]
59. Luo, Y.; Wang, J.; Yang, L.; Gao, T.; Pei, R. In vitro selection of DNA aptamers for the development of fluorescent aptasensor for sarcosine detection. *Sens. Actuat. B Chem.* **2018**, *276*, 128–135. [[CrossRef](#)]
60. Rakhi, R.B.; Nayak, P.; Xia, C.; Alshareef, H.N. Novel amperometric glucose biosensor based on MXene nanocomposite. *Sci. Rep.* **2016**, *6*, 36422. [[CrossRef](#)]
61. Wang, F.; Yang, C.; Duan, M.; Tang, Y.; Zhu, J. TiO₂ nanoparticle modified organ-like Ti₃C₂ MXene nanocomposite encapsulating hemoglobin for a mediator-free biosensor with excellent performances. *Biosens. Bioelectron.* **2015**, *74*, 1022–1028. [[CrossRef](#)]
62. Wang, H.; Wu, Y.; Zhang, J.; Li, G.; Huang, H.; Zhang, X.; Jiang, Q. Enhancement of the electrical properties of MXene Ti₃C₂ nanosheets by post-treatments of alkalization and calcination. *Mater. Lett.* **2015**, *160*, 537–540. [[CrossRef](#)]
63. Zheng, J.; Diao, J.; Jin, Y.; Ding, A.; Wang, B.; Wu, L.; Weng, B.; Chen, J. An Inkjet Printed Ti₃C₂-GO Electrode for the Electrochemical Sensing of Hydrogen Peroxide. *J. Electrochem. Soc.* **2018**, *165*, B227–B231. [[CrossRef](#)]
64. Lorencova, L.; Bertok, T.; Filip, J.; Jerigova, M.; Velic, D.; Kasak, P.; Mahmoud, K.A.; Tkac, J. Highly stable Ti₃C₂T_x(MXene)/Pt nanoparticles-modified glassy carbon electrode for H₂O₂ and small molecules sensing applications. *Sens. Actuat. B Chem.* **2018**, *263*, 360–368. [[CrossRef](#)]
65. Xu, B.; Zhu, M.; Zhang, W.; Zhen, X.; Pei, Z.; Xue, Q.; Zhi, C.; Shi, P. Ultrathin MXene-Micropattern-Based Field-Effect Transistor for Probing Neural Activity. *Adv. Mater.* **2016**, *28*, 3333–3339. [[CrossRef](#)]
66. Fang, Y.; Yang, X.; Chen, T.; Xu, G.; Liu, M.; Liu, J.; Xu, Y. Two-dimensional titanium carbide (MXene)-based solid-state electrochemiluminescent sensor for label-free single-nucleotide mismatch discrimination in human urine. *Sens. Actuat. B Chem.* **2018**, *263*, 400–407. [[CrossRef](#)]
67. Wu, L.; Lu, X.; Dhanjai; Wu, Z.S.; Dong, Y.; Wang, X.; Zheng, S.; Chen, J. 2D transition metal carbide MXene as a robust biosensing platform for enzyme immobilization and ultrasensitive detection of phenol. *Biosens. Bioelectron.* **2018**, *107*, 69–75. [[CrossRef](#)] [[PubMed](#)]
68. Zhu, X.; Liu, B.; Hou, H.; Huang, Z.; Zeinu, K.M.; Huang, L.; Yuan, X.; Guo, D.; Hu, J.; Yang, J. Alkaline intercalation of Ti₃C₂ MXene for simultaneous electrochemical detection of Cd(II), Pb(II), Cu(II) and Hg(II). *Electrochim. Acta* **2017**, *248*, 46–57. [[CrossRef](#)]
69. Rasheed, P.A.; Pandey, R.P.; Rasool, K.; Mahmoud, K.A. Ultra-sensitive electrocatalytic detection of bromate in drinking water based on Nafion/Ti₃C₂T_x (MXene) modified glassy carbon electrode. *Sens. Actuat. B Chem.* **2018**, *265*, 652–659. [[CrossRef](#)]
70. Zhou, L.; Zhang, X.; Ma, L.; Gao, J.; Jiang, Y. Acetylcholinesterase/chitosan-transition metal carbides nanocomposites-based biosensor for the organophosphate pesticides detection. *Biochem. Eng. J.* **2017**, *128*, 243–249. [[CrossRef](#)]
71. Sinha, A.K.; Dhanjai; Mugo, S.M.; Chen, J.; Lokesh, K.S. MXene-based sensors and biosensors: Next-generation detection platforms. In *Handbook of Nanomaterials in Analytical Chemistry*; Elsevier: Amsterdam, The Netherlands, 2020; pp. 361–372.

Disclaimer/Publisher's Note: The statements, opinions and data contained in all publications are solely those of the individual author(s) and contributor(s) and not of MDPI and/or the editor(s). MDPI and/or the editor(s) disclaim responsibility for any injury to people or property resulting from any ideas, methods, instructions or products referred to in the content.